Robust Tracking Control for Non-holonomic Wheeled Mobile Robots in a Leader-Follower Formation with Time-gap Separation

Mauro Baquero-Suárez
Instituto Tecnológico de Buenos Aires
(ITBA)
CONICET
Buenos Aires, Argentina
mbaquero@itba.edu.ar

Ignacio Mas
Instituto Tecnológico de Buenos Aires
(ITBA)
CONICET
Buenos Aires, Argentina
imas@itba.edu.ar

Juan I. Giribet
Universidad de Buenos Aires
Facultad de Ingeniería
Instituto Argentino de Matemática
CONICET
Buenos Aires, Argentina
jgiribet@fi.uba.ar

***Abstract*—This work addresses the design and validation of a time-gap synchronized leader-follower formation scheme for wheeled mobile multi-robot systems. This scheme generates reference trajectories for each robot through the estimation via observer of the delayed behavior of its predecessor. A second goal of this paper is the precise and efficient tracking of these references to achieve the desired movement of the chained formation. Therefore, a robust two-stage controller is proposed, where the angular velocity of lateral wheels is regulated in a first stage by a torque controller, with velocity references provided by a tracking controller that commands the robot's pose in a second stage. The outlined theory is validated through successful results in simulations of multi-body dynamic models, integrating ADAMS and MATLAB.**

***Index Terms*—Mobile Robots, Robust Control, Leader-follower Formations, Multi-body Dynamics.**

I. Introduction

Nowadays, mobile robotics is one of most popular research topics, due to the wide range of possible applications. Particularly, mobile multi-robot systems have attracted the research community due to several advantages obtained with synchronized vehicles such as flexible reconfigurability, diverse functionality, and increased coverage, which are appreciable in recent developments (see [1]–[3]). Within this context, the main aim of this paper is focused on presenting a way to synchronize the movement of a chained wheeled n-robot system. Therefore, a Time-gap Leader-follower formation (TLF) methodology is employed for achieving this synchronization, where an arbitrary reference trajectory can be built to be tracked by a leader robot $\{1\}$, and the others $n-1$ are delayed followers of $\{1\}$ that use adjustable time-gap separations to remain at a desired proximity. TLF consists in the inclusion of a non-linear observer for estimating the delayed behavior of each robot in the formation, and using it as reference trajectories for subsequent robot. It differs from other techniques such as the leader-follower scheme [4], where the pose of each robot is regulated as a function of the distance between them. TLF governs the time instead of such distance and consequently varies the velocity of each vehicle to ensure the desired time-gap. Potential advantages include better reaction responses of follower robots over unexpected deviation maneuvers by leader robots to avoid collisions with detected obstacles.

On the other hand, high precision and robustness are demanded in the tracking of reference trajectories generated by TLF. Therefore, some concepts of robust and non-linear control are appropriated here to design a two-stage controller (two control loops in cascade) that governs the behavior of wheeled non-holonomic mobile robots, by conveniently dividing velocity regulation and trajectory tracking. Thus, an angular velocity controller (AVC) is designed in a first stage, from a simple lumped-parameter model that describes the dynamics of each lateral wheel. It allows to independently regulate the rotation of these wheels through a SISO classical linear control structure that provides the needed input torque on their gyro axes. Then, a non-linear tracking controller (TC) is proposed in a second stage, based on Lyapunov redesign, to ensure robust tracking of reference trajectories and rejection of side slipping disturbances associated to the kinematic model. Successful results obtained in realistic simulations validate the effectiveness of the whole control system.

Regarding the developed realistic simulations, ADAMS was used because of its capability to generate a detailed simulation for the behavior of rigid and/or flexible multi-body dynamic systems (see [5]–[7]). So, a virtual dynamic plant of several differential mobile robots was built in ADAMS/View to include the more relevant dynamics that affect these vehicles in a real world environment. This plant was linked to MATLAB/Simulink in simulation run-time, where the two-stage controller and TLF were suitably implemented.

The structure of this paper from this point ahead is arranged such that Section II describes the kinematic and dynamic model of the mobile robot built on ADAMS. Section III encompasses the formulation of the robust two-stage tracking controller. Section IV reveals the TLF methodology for multi-robot trajectory generation. Section V exhibits the obtained results in simulations with three and five robots, and finally Section VI gives some concluding remarks.

II. Robot Modeling

A. Kinematic model

An idealized model of a differential-drive wheeled mobile robot is exhibited in Fig. 1, with a distance L between the point-contact of their assumed knife edge lateral wheels, and a rotation axis center located at point c, where the body reference frame $\{x_b, y_b\}$ is defined. Lateral wheels of this non-holonomic vehicle have radius R, and they are commonly actuated by a torque applied around their giro axes. The robot's center of mass cm is displaced behind point c by certain unknown distance d, improving the vehicle's stability and maneuvering conditions. A rear castor wheel serves as a support point-contact to balance the weight distribution. When the robot is in motion, its position with respect to the inertial frame $\{\chi, \gamma\}$ is given by $\{x, y\}$ variables, while its orientation is provided by angle θ. So, it moves on a planar surface by generating a trajectory p that depends on the linear velocities $v_r = \omega_r R$ and $v_l = \omega_l R$, where ω_r and ω_l are the angular velocities of right and left wheels.

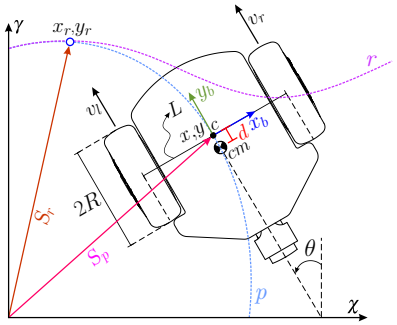

Fig. 1: Kinematics of a two-wheeled non-holonomic mobile robot.

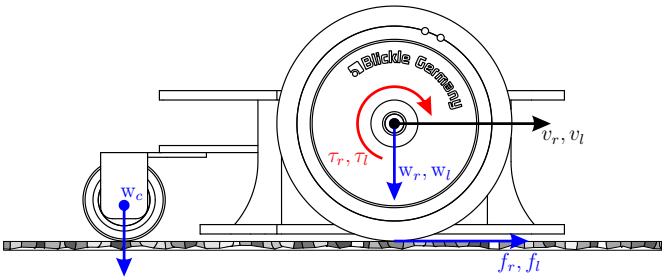

Fig. 2: Free-body diagram of the mobile robot. Subscripts r and l mean the vehicle's right and left sides.

The kinematic model of this system is then:

$$\begin{bmatrix}\dot{x}\\ \dot{y}\\ \dot{\theta}\end{bmatrix} = \begin{bmatrix}-u_1 \sin\theta\\ u_1 \cos\theta\\ u_2\end{bmatrix}, \quad \begin{bmatrix}u_1\\ u_2\end{bmatrix} = \overbrace{\begin{bmatrix}R/2 & R/2\\ -R/L & R/L\end{bmatrix}}^{S_\omega} \begin{bmatrix}\omega_l\\ \omega_r\end{bmatrix}, \quad (1)$$

where u_1 and u_2 correspond to the robot's linear and angular velocities at point c, and they are related to the wheels' angular velocities by matrix S_ω. Then, the control objective is to regulate u_1 and u_2, for achieving a robust and efficient tracking of reference trajectories such as r in Fig. 1.

B. Dynamic model

Although Lagrangian-based dynamic models are commonly stated for these robots, we considered for simplicity to separately model the traction dynamics of the actuated lateral wheels[1]. Thus, Fig. 2 is considered for the wheels' traction dynamics, in which lumped forces and momentum have been defined at their giro axes and contact-points with the floor (assuming that the robot moves on a flat surface). So, w_r, w_l and w_c represent the forces associated to the vehicle's weight distribution that act on the wheels' axes, whose relationship with the total weight is assumed as $0.8m_t = \frac{w_r}{g} + \frac{w_l}{g}$, and $0.2m_t = \frac{w_c}{g}$ (see Table I for m_t and g). τ_r and τ_l are the applied torques to lateral wheels or control inputs, while f_r and f_l depict their exerted friction forces by the reaction with the road surface, when moving at certain linear velocity v_r and v_l. Then, by Newton's balanced forces and momentum laws on Fig. 2, a lumped-parameter model is derived as

$$f_{\{r,l\}} = \frac{w_{\{r,l\}}}{g}\dot{v}_{\{r,l\}}, \quad (2)$$

$$\tau_{\{r,l\}} = R f_{\{r,l\}} + \underbrace{\frac{J\dot{v}_{\{r,l\}}}{R}}_{J\dot{\omega}_{\{r,l\}}} + T_{f\{r,l\}}, \quad (3)$$

$$\mu_{roll} = \frac{f_{\{r,l\}}}{f_{n\{r,l\}}}, \quad (4)$$

where $\{r, l\}$ stands for right wheel or left wheel, J is the moment of inertia, μ_{roll} is the assumed-constant rolling friction coefficient (J and μ_{roll} are supposed equal for both wheels), f_n is the normal force, which is proportional to the angular acceleration of each wheel, and T_f is the friction torque on wheels' giro axes, which is considered as an input disturbance.

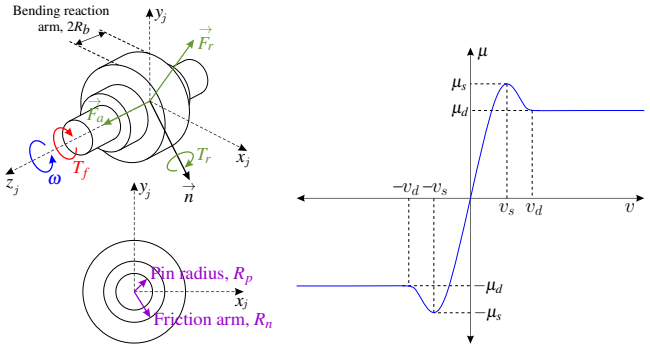

(a) Free-body diagram of wheels' revolute joints.

(b) Friction coefficient as a function of wheel's linear velocity.

Fig. 3: Frictional torque dynamics for each wheel.

Consequently to the robot's motion-resistant, T_f appears due to each wheel's angular velocity. Therefore, its dynamics is modeled by the following non-linear expression:

$$T_f = \mu\left[R_n |F_a| + R_p\sqrt{F_{r_{x_j}}^2 + F_{r_{y_j}}^2} + \frac{R_p}{R_b}T_r + T_{\text{pre}}\right]. \quad (5)$$

[1]One advantage is that derived equations allow to design a linear control system in Subec III-A that adequately governs the behavior of both wheels.

Each term in (5) has its representation in Fig. 3(a), where F_a and F_r are the joint reaction forces, T_r is the bending moment in the $\vec{n}$ direction, R_p, R_n, and R_b are the corresponding pin radius, friction arm, and bending reaction arm. T_{pre} is a preload torque and μ depicts the friction coefficient, whose value varies depending on three friction regimes (static friction, dynamic friction, and a transition state between both) and the joint's linear velocity transitions $v_s = R\omega_s$ and $v_d = R\omega_d$ as Fig. 3(b) shows, being ω_s and ω_d the angular velocity transitions.

C. Virtual dynamic model built in ADAMS™software

According to Subsections II-A and II-B, a virtual plant of mobile robots was built in ADAMS, characterized by the parameters in Table I. Fig. 4 shows a top view of one virtual robot in ADAMS/View environment[2], which is a multi-body dynamic system constituted by a chassis, two lateral wheels and a castor wheel rear mechanism, and they are connected by revolute joints. Besides, a flat and rigid surface represents the road, whose reaction contact forces with the vehicle's wheels were also modeled by the contact force parameters of Table I. This virtual model is exported to MATLAB/Simulink as a MIMO non-linear plant for developing cooperative simulations, where control systems can be easily programmed on Simulink's graphical structure, to command the ADAMS model through their input and output variables.

Table I: Parameters of the mobile robot.

Physical properties of the mobile robot				
Total mass	m_t	1.245 kg		
Radius of lateral wheels	R	50 mm		
Distance between lateral wheels	L	156 mm		
Mass moment of inertia of lateral wheels	J	52.91 kg · mm^2		
Offset distance of center of mass	d	unknown		
Gravity	g	9.807 m/s^2		
Parameters to model friction into robot's joints				
Parameters		Lateral wheels	Castor wheel	Steering of castor wheel
Static friction coefficient	μ_s	0.15	0.15	0.05
Dynamic friction coefficient	μ_d	0.1	0.1	0.033
Friction arm	R_n	12 mm	6.2 mm	2.5 mm
Pin radius	R_p	8 mm	3.025 mm	2.5 mm
Bending reaction arm	R_b	36 mm	30 mm	3 mm
Stiction transition velocity	v_s	1 mm/s	1 mm/s	1 mm/s
Dynamic transition velocity	v_d	$1.5v_s$	$1.5v_s$	$1.5v_s$
Friction torque preload	T_{pre}	0.0 N · mm	0.0 N · mm	0.0 N · mm
Switched effects in friction model				
Effect		Lateral wheels	Castor wheel	Steering of castor wheel
Reaction force		On	On	On
Preload		Off	Off	Off
Bending moment		On	On	On
Inactive during static		Off	Off	Off
Contact force parameters for the wheels				
Impact force parameters				
Stiffness	10 N/mm			
Force exponent	2.2			
Damping	0.2 N · sec/mm			
Penetration depth	1×10^{-3} mm			
Coulomb friction parameters				
Static friction coefficient	μ_{sf}	7.3×10^{-2}		
Dynamic friction coefficient	μ_{df}	5.5×10^{-2}		
Stiction transition velocity	v_{sf}	2 mm/s		
Friction transition velocity	v_{df}	3 mm/s		

III. Control System Formulations

Trajectory tracking for each robot in the formation is achieved through the two-stage control system exhibited in Fig 5. In the first stage, an angular velocity controller (AVC) is designed for each lateral wheel, based on the previously described traction model and certain known information about uncertainty and disturbing dynamics on it. The second stage implements a tracking controller (TC) that ensures robust tracking of reference trajectories in the vehicle. Computed control actions in TC serve as the input angular velocity references of AVC, which provides the needed torque to the lateral wheels' axes to regulate these desired velocities.

[2]This block exhibits that angle θ is unavailable as output, therefore an extended Kalman filter (EKF) will be used to estimate it.

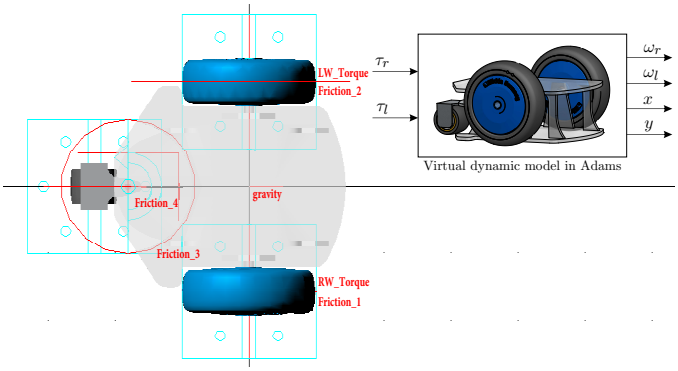

Fig. 4: Multi-body dynamic model of the mobile robot.

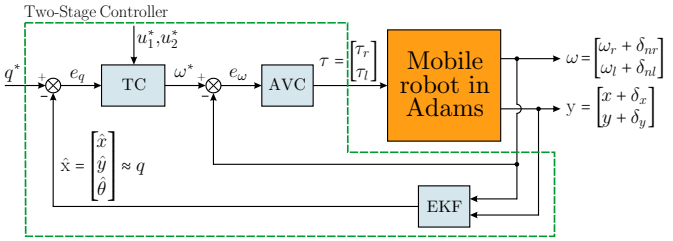

Fig. 5: Control system for each robot in the formation.

A. Angular velocity controller (AVC) for lateral wheels

From (2) and (3), the traction model for each lateral wheel is rewritten as

$$\dot{\omega} = \frac{1}{\left(\frac{\text{w}R^2}{g} + J\right)}(\tau - T_f) = \kappa(\tau - T_f), \tag{6}$$

where κ is a constant that accompanies the control input τ, and T_f is the non-linear disturbance considered as an unknown function, but continuous in $\mathbb{R}$ and absolutely bounded, $|T_f| \leq \rho$. Uncertainty on κ suggests that (6) be rewritten with its known nominal term $\hat{\kappa}$ as follows:

$$\dot{\omega} = \hat{\kappa}\left(1 + \frac{\kappa - \hat{\kappa}}{\hat{\kappa}}\right)\tau - \overbrace{\kappa T_f}^{\xi}. \tag{7}$$

Remark 1: Observe that it is convenient to redefine the traction model (7) in the frequency domain as a set of models $\mathcal{G}$ parametrized by a nominal model $G_0(s)$, a weight transfer function $W_\delta(s)$ associated to uncertainty features and multiplied by an uncertainty bound $\Delta \in \mathbb{C}$, and the additive non-linear disturbance ξ at the input. That is,

$$\mathcal{G} = \{G_0(s)[1 + W_\delta(s)\Delta],\ \|\Delta\|_2 \leq 1\}, \tag{8}$$

where the nominal model is defined as $G_0(s) = \frac{\hat{\kappa}}{s}$, and $W_\delta(s)$ must be designed to cover the uncertainty $\left(\frac{\kappa-\hat{\kappa}}{\hat{\kappa}}\right)$ for all frequencies, where its ultimate bound is assumed to be in the ball $B_\Delta = \{\|\Delta\|_2 \leq 1\}$. The κ parameter has a dynamic uncertainty on its bound that is unknown at high frequencies, where angular accelerations and vehicle orientation produce unmodeled dynamics in μ_{roll} and f definitions. This justifies the selection of the set $\mathcal{G}$ for the traction dynamics[3].

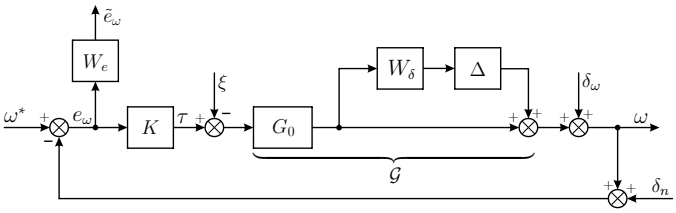

Fig. 6: Blocks diagram of control system for AVC stage.

Fig. 6 shows the structure of the AVC stage, where ω^* is the angular velocity reference, δ_ω and δ_n represent the associated disturbances to measuring error and noise at the output ω, ξ is the disturbing friction torque at the input τ, and terms W_δ and W_e are weighting transfer functions to bound the model uncertainty distribution and the tracking error energy for all frequencies ($\forall w$). That said, the following necessary conditions for robust stability and robust performance must be satisfied:

- For robust stability, a controller $K(s)$ is capable to stabilize the whole set of models $\mathcal{G}$, if satisfies the following necessary condition:

$$\|W_\delta(s)T(s)\|_\infty = \sup_{jw} |W_\delta(jw)T(jw)| < 1 \ \forall w, \quad (9)$$

being $T(s) = G_0(s)K(s)/[1 + G_0(s)K(s)]$ the complementary sensitivity function of the closed-loop control system.

- By defining the performance as the attenuation of tracking error energy (weighted by $W_e(s)$) of certain set of reference signals $r(t)$, then, the controller $K(s)$ must satisfy the following necessary condition for nominal performance:

$$\|W_e(s)S(s)\|_\infty = \sup_{jw} |W_e(jw)S(jw)| < 1 \ \forall w, \quad (10)$$

where $S(s) = 1/[1 + G_0(s)K(s)]$ is the sensitivity function of the closed-loop control system. It allows to also define the necessary condition for robust performance as follows:

$$\sup_{jw}\{|W_e(jw)S(jw)| + |W_\delta(jw)T(jw)|\} < 1 \ \forall w. \quad (11)$$

Hence, based on previous experience on traction dynamics, the two weighting function candidates are selected as

$$W_\delta(s) = \frac{s + 1.27}{2.54} \ \text{ and } \ W_e(s) = \frac{s + 0.1}{1.5s}, \quad (12)$$

[3]Uncertainty characterization into frequency domain allows to distinguish a range inwhich it significantly affects to nominal model. Then, a robust control can be designed with a specific and efficient bandwidth to compensate it.

where robust stability would be guaranteed with a 50% relative error of $\hat{\kappa}$ parameter, up to 2.12 rad/s, and performance would be conditioned at least to the robust tracking of step-references in spite of all kind of bounded disturbances ξ and δ_ω ($\|\xi(s)\|_2 < \alpha_1$ and $\|\delta_\omega(s)\|_2 < \alpha_2$), until 0.09 rad/s. Then, controller $K(s)$ was designed by the single-input single-output (SISO) loop shaping method to satisfy stability and performance conditions (9), (10), and (11). According to this method, the following linear controller is proposed:

$$K(s) = \frac{150\left(s^2 + 3s + 0.3025\right)}{s\,(s+2)} \approx 150 + \frac{22}{s} + \frac{128}{s+2}, \quad (13)$$

which shapes the nominal internal loop $L(s) = G_0(s)K(s)$ to be located into the delimited zone between $W_e(s)$ and $1/W_\delta(s)$ at low and high frequencies as Fig. 7(a) shows. So, the control system attenuates ξ and δ_ω until approximately 0.189 rad/s, and its closed-loop bandwidth attenuates in turn the noise δ_n at the output. This controller allows that conditions (9), (10), and (11) be satisfied such as Fig. 7(b) exhibits, and its integral action ensures zero-velocity-error in the tracking of any ramp-reference, with an anti-windup scheme that handles actuator saturation[4].

Finally, robustness of AVC was validated by an experimental nyquist diagram on the open loop control system L, where a modulus margin value $\Delta_\text{M} \approx 0.81$ is found by measuring the distance between the point $[-1, 0]$ and the nyquist plot as Fig. 7(c) shows. This parameter allows to quantify stability margins of AVC on the virtual dynamic model, and its larger value than 0.5 is enough to say that control system is robust. This nyquist plot was obtained by using a sufficiently excited pseudo-random binary signal (PRBS) as the reference ω^* and a digital implementation of (13) for AVC. Then, data for error e_ω and output ω were collected and used to generate the frequency-domain representation of L through Fourier analysis and non-parametric identification methods (see [8], [9]).

B. Tracking controller (TC) for one robot

Consider the following disturbed kinematic model:

$$\begin{bmatrix} \dot{x} \\ \dot{y} \\ \dot{\theta} \end{bmatrix} = \begin{bmatrix} -\sin\theta & 0 \\ \cos\theta & 0 \\ 0 & 1 \end{bmatrix} \begin{bmatrix} u_1 + \delta_1 \\ u_2 + \delta_2 \end{bmatrix}. \quad (14)$$

Remark 2: Note that (14) is the extended model of (1), where additive disturbances δ_1 and δ_2 have been included to involve the slipping effect of lateral wheels when in motion. Although these disturbances are unknown, they are assumed as continuous and absolutely bounded functions in $\mathbb{R}$, and their bounds are perfectly known.

For the tracking problem, a reference trajectory $q^* = [x^*\ y^*\ \theta^*]^\text{T}$ must be followed by the robot trajectory $q = [x\ y\ \theta]^\text{T}$. Then, an ideal reference robot could be imagined by generating q^*, through the following kinematic model:

[4]The operation range for the actuators were settled from -15 N·mm to 15 N·mm.

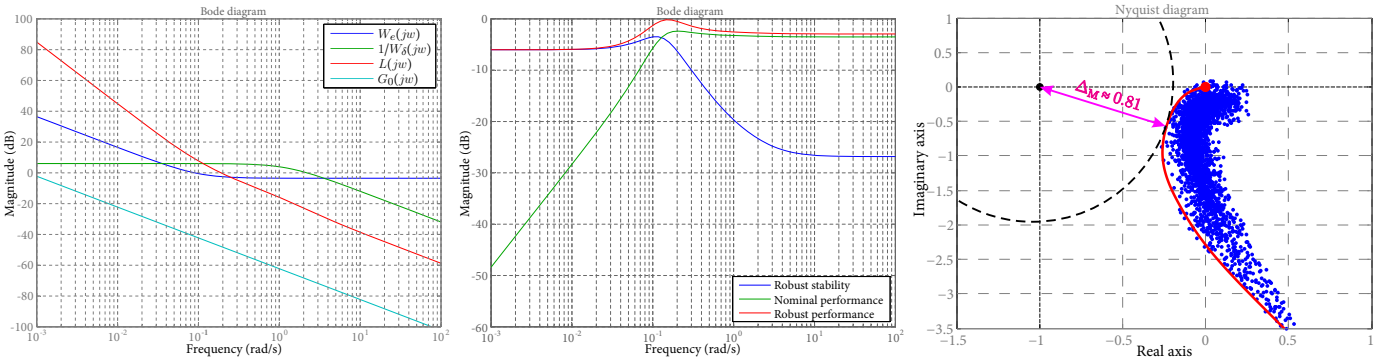

(a) Shaping of the loop $L(s)$. (b) Verification of robust conditions. (c) Experimental nyquist diagram of $L(s)$.

Fig. 7: Loop shaping method for tuning AVC.

$$\begin{bmatrix} \dot{x}^* \\ \dot{y}^* \\ \dot{\theta}^* \end{bmatrix} = \begin{bmatrix} -\sin\theta^* & 0 \\ \cos\theta^* & 0 \\ 0 & 1 \end{bmatrix} \begin{bmatrix} u_1^* \\ u_2^* \end{bmatrix}, \tag{15}$$

where u_1^* and u_2^* are the kinematic control variables of reference robot, i.e. the desired time-variant values of linear and angular velocities to generate q^*. Hence, a feedback control law $[u_1\ u_2]^{\mathrm{T}} = u(q, q^*, u_1^*, u_2^*)$ could be designed such that tracking error $e_q = q^* - q$ effectively converges to zero, in spite of slip disturbances in (14). For this reason, a robust controller based on Lyapunov redesign is proposed here, by taken into consideration the following assumptions:

Assumption 1: Kinematic variables u_1^* and u_2^*, are completely available and absolutely bounded.

Assumption 2: Reference trajectories are established in such a way that u_1^* and u_2^* do not go to zero simultaneously until the robot reaches a desired final pose.

Besides, a tracking error model is necessarily defined as

$$\overbrace{\begin{bmatrix} e_1 \\ e_2 \\ e_3 \end{bmatrix}}^{{}^{b}e_q} = \overbrace{\begin{bmatrix} -\sin\theta & \cos\theta & 0 \\ \cos\theta & \sin\theta & 0 \\ 0 & 0 & 1 \end{bmatrix}}^{S_e} \overbrace{\begin{bmatrix} x^* - x \\ y^* - y \\ \theta^* - \theta \end{bmatrix}}^{e_q}, \tag{16}$$

where e_q is conveniently expressed in a frame related with the body frame $\{x_b, y_b\}$ through non-singular matrix S_e (which in this case it is not only a rotation, because the axes were redefined), for achieving an independent tracking error dynamics from inertial frame $\{\chi, \gamma\}$. Then, the derivative of (16) with respect to time is computed to obtain the following differential equations:

$$\begin{aligned} \dot{e_1} &= -e_2(u_2 + \delta_2) + u_1^* \cos e_3 - (u_1 + \delta_1), \\ \dot{e_2} &= e_1(u_2 + \delta_2) - u_1^* \sin e_3, \\ \dot{e_3} &= u_2^* - (u_2 + \delta_2), \end{aligned} \tag{17}$$

which are used by Lyapunov redesign as outlined below.

1) Lyapunov redesign: Firstly, a nominal controller based on Lyapunov theorem is designed such that the tracking errors vector ${}^{b}e_q$ without slip disturbances, asymptotically converges to the origin. Then, this nominal controller is redesigned by adding another complementary non-linear term to tackle these assumed disturbances and consolidate the asymptotic stability of closed-loop control system. In this way, the following nominal controller is proposed.

Proposition 1 (Nominal controller design): Given the following tracking error dynamical equations without slip disturbances:

$$\begin{aligned} \dot{e_1} &= -e_2\bar{u}_2 + u_1^* \cos e_3 - \bar{u}_1, \\ \dot{e_2} &= e_1\bar{u}_2 - u_1^* \sin e_3, \\ \dot{e_3} &= u_2^* - \bar{u}_2, \end{aligned} \tag{18}$$

then, a nonlinear control law is proposed for (18) as follows:

$$\begin{aligned} \bar{u}_1 &= k_1 e_1 + u_1^* \cos e_3, \\ \bar{u}_2 &= \frac{k_2}{k_3} \sin e_3 + u_2^* - \frac{e_2 u_1^*}{k_3}, \end{aligned} \tag{19}$$

with the arbitrarily chosen gains k_1, k_2, and k_3 as positive constants to ensure asymptotic stability into the domain $\mathcal{D} = \{\forall\, [e_1\ e_2\ e_3]^{\mathrm{T}} \in \mathbb{R}^3 : -\pi < e_3 < \pi\}$ where the tracking error trajectories converge to zero.

Proof 1: For the sake of brevity, the proof is not included here, but it directly follows the steps of [10]. □

Remark 3: Note that the following closed-loop dynamical system (control law (19) applied to (18)):

$$\begin{aligned} \dot{e_1} &= -\frac{e_2}{k_3}\left(k_2 \sin e_3 - e_2 u_1^* + k_3 u_2^*\right) - k_1 e_1, \\ \dot{e_2} &= \frac{e_1}{k_3}\left(k_2 \sin e_3 - e_2 u_1^* + k_3 u_2^*\right) - u_1^* \sin e_3, \\ \dot{e_3} &= -\frac{1}{k_3}\left(k_2 \sin e_3 - e_2 u_1^*\right), \end{aligned} \tag{20}$$

has an infinite set of equilibrium points $\mathcal{E} = \{[e_1\ e_2\ e_3]^{\mathrm{T}} = [0\ 0\ j\pi]^{\mathrm{T}} : j \in \mathbb{Z}\}$, and it is easy to see that those with an odd number in j are unstable. Therefore, according to Prop. 1, trajectories of tracking error vector ${}^{b}e_q$ into any domain such that $(j-2)\,\pi < e_3 < j\pi$ will converge to the origin $(j-1)\,\pi$, $\forall j(\text{odd}) \in \mathbb{Z}$. Unstable points of $j\pi$ are named as singular values of the control system.

Control gains are settled as $k_1 = 0.23$, $k_2 = 0.83$ and $k_3 = 12\text{E}3$, to guarantee a convergence for tracking error

trajectories as Fig. 8 exhibits. Then, complementary control law is proposed below to give robustness to the closed-loop control system.

Proposition 2 (Complementary control law): Given that the nominal control law $[\bar{u}_1\ \bar{u}_2]^{\mathrm{T}}$ succeeded in achieving the asymptotic stability of nominal system (18) in the domain $\mathcal{D}$, then, a complementary control law is designed as follows:

$$\begin{bmatrix} \varrho_1 \\ \varrho_2 \end{bmatrix} = \begin{cases} -\eta\,\mathrm{sign}\,(\boldsymbol{\lambda}), & \text{if} \quad \eta\,\|\boldsymbol{\lambda}\|_1 \geq \epsilon, \\ -\frac{\eta^2\boldsymbol{\lambda}}{\epsilon}, & \text{if} \quad \eta\,\|\boldsymbol{\lambda}\|_1 < \epsilon, \end{cases} \tag{21}$$

with $\eta \geq \|[\delta_1\ \delta_2]\|_\infty$ and $\boldsymbol{\lambda} = [-e_1\ -k_3 \sin e_3]^{\mathrm{T}}$, so that the overall continuous control $[u_1\ u_2]^{\mathrm{T}} = [\bar{u}_1+\varrho_1\ \bar{u}_2+\varrho_2]^{\mathrm{T}}$ achieves robust stabilization of the closed-loop system by ensuring that all tracking error trajectories in $\mathcal{D}$ will be confined into a small bounded ball that is function of ϵ (with its center in the origin) and forced to remain there in the presence of slip disturbances.

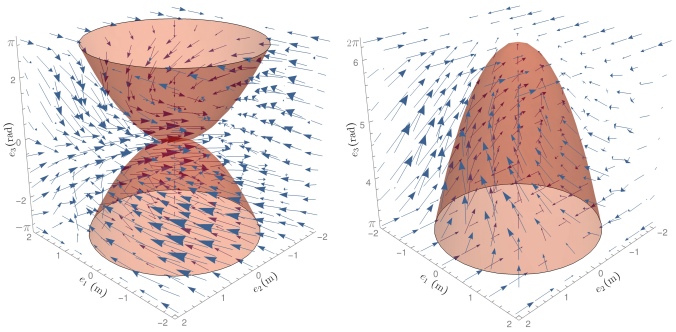

Fig. 8: Behavior of tracking error trajectories around equilibrium points $[0\,0\,0]^{\mathrm{T}}$ and $[0\,0\,2\pi]^{\mathrm{T}}$.

Proof 2: Consider (17) arranged as $\dot{e} = f(e)+g(e)(u+\delta)$, with $f(e) = \begin{bmatrix} u_1^* \cos e_3 & -u_1^* \sin e_3 & u_2^* \end{bmatrix}^{\mathrm{T}}$, $u = \begin{bmatrix} u_1 & u_2 \end{bmatrix}^{\mathrm{T}}$, $g(e) = \begin{bmatrix} -1 & -e_2 \\ 0 & e_1 \\ 0 & -1 \end{bmatrix}$, and $\delta = \begin{bmatrix} \delta_1 & \delta_2 \end{bmatrix}^{\mathrm{T}}$. Then, a Lyapunov candidate function is selected as $V_1 = \frac{1}{2}(e_1^2+e_2^2)+k_3\,(1-\cos e_3)$, whose time derivative along (17) results as follows:

$$\dot{V}_1 = -k_1 e_1^2 - k_2 \sin^2 e_3 + \boldsymbol{\lambda}^{\mathrm{T}}\delta + \boldsymbol{\lambda}^{\mathrm{T}}\varrho, \tag{22}$$

where $\boldsymbol{\lambda}^{\mathrm{T}} = \frac{\partial V_1}{\partial e} g(e) = [-e_1\ -k_3 \sin e_3]$ and $\varrho = [\varrho_1\ \varrho_2]^{\mathrm{T}}$ is the control law (21). Given that bounds of δ_1 and δ_2 are assumed known, then $\|\delta\|_\infty \leq \beta$, with β also known, and $\dot{V}_1$ is bounded by the following inequality:

$$\dot{V}_1 \leq \boldsymbol{\lambda}^{\mathrm{T}}\delta + \boldsymbol{\lambda}^{\mathrm{T}}\varrho \leq \|\boldsymbol{\lambda}\|_1 \|\delta\|_\infty + \boldsymbol{\lambda}^{\mathrm{T}}\varrho. \tag{23}$$

In order to cancel δ, control law ϱ is proposed as (21) specifies, with $\eta \geq \beta$. In consequence, for the case when $\eta\,\|\boldsymbol{\lambda}\|_1 \geq \epsilon$ the following expression is obtained:

$$\dot{V}_1 \leq \|\boldsymbol{\lambda}\|_1 \|\delta\|_\infty - \eta\,\|\boldsymbol{\lambda}\|_1 \leq (\beta-\eta)\,\|\boldsymbol{\lambda}\|_1 \leq 0. \tag{24}$$

So, $\beta\,\|\boldsymbol{\lambda}\|_1 \leq \eta\,\|\boldsymbol{\lambda}\|_1$, and $\dot{V}_1$ remains a negative semi-definite and uniformly continuous function so that $\dot{V}_1 \to 0$ as $t \to \infty$, and tracking error solutions are forced to the origin in spite of disturbances. Finally, in the case $\eta\,\|\boldsymbol{\lambda}\|_1 < \epsilon$ results the following inequality:

$$\dot{V}_1 \leq \beta\,\|\boldsymbol{\lambda}\|_1 - \frac{\eta^2\,\|\boldsymbol{\lambda}\|_1^2}{\epsilon} \leq \eta\,\|\boldsymbol{\lambda}\|_1 - \frac{\eta^2\,\|\boldsymbol{\lambda}\|_1^2}{\epsilon} \leq \frac{\epsilon}{4}, \tag{25}$$

where $\epsilon/4$ is the maximum value of $\dot{V}_1$. Then, from (22) and (25) is deduced that $\dot{V}_1$ satisfies

$$\dot{V}_1 \leq -k_1 e_1^2 - k_2 \sin^2 e_3 + \frac{\epsilon}{4} \leq -\underline{k}\,\left\|{}^b e_q\right\|_2^2 + \frac{\epsilon}{4}, \tag{26}$$

with $\underline{k} = \min\{k_1, k_2\}$, which yields

$$\dot{V}_1 \leq \overbrace{-\underline{k}\,(1-\phi)\,\left\|{}^b e_q\right\|_2^2}^{-\alpha(\left\|{}^b e_q\right\|_2)} \text{ if } -\underline{k}\phi\,\left\|{}^b e_q\right\|_2^2 + \frac{\epsilon}{4} \leq 0, \tag{27}$$

with $0 < \phi < 1$. Hence $\dot{V}_1 \leq -\alpha(\left\|{}^b e_q\right\|_2)$ for $\left\|{}^b e_q\right\|_2 \geq \sqrt{\frac{\epsilon}{4\underline{k}\phi}} = \varsigma(\epsilon)$. It guarantees an uniform ultimate boundedness for the closed-loop control system, where the tracking error solutions e_1, e_2 and e_3 will be forced to remains into the ball $B_\varsigma = \{\left\|{}^b e_q\right\|_2 \leq \varsigma\}$ in spite of δ_1 and δ_2, and ultimate bound ς will be as small as ϵ be reduced. □

Control law $[\varrho_1\ \varrho_2]^{\mathrm{T}}$ is a continuous approximation of the discontinuous function sign$(\cdot)$, which avoids some problems such as chattering phenomenon and fluctuations in the control response due to switching imperfections that discontinuous ones cause in practical applications. Additionally, as Remark 3 explains, closed-loop dynamics are repetitive each 2π radians along e_3, therefore, robustness of TC holds regardless of changes of the origin location. On the other hand, given that the unavailable robot's orientation θ is used for TC (see Fig. 4), the EKF is implemented to estimate it based on the robot position and control inputs. Simulations with virtual multi-robot dynamic models are presented in Section V, where implementation of TC uses $\eta = 1.9\mathrm{E}^{-3}$ and $\epsilon = 0.1$ for all robots, showing good performance[5].

C. Extended Kalman filtering (EKF)

Given that angle θ can be adequately estimated from other known variables, such as measured distances x and y, then, an odometry-based motion model[6] is prescribed as

$$\overbrace{\begin{bmatrix} x_i \\ y_i \\ \theta_i \end{bmatrix}}^{\mathrm{x_i}} = \overbrace{\begin{bmatrix} x_{i-1} - u_{1,i}\sin\theta_i \\ y_{i-1} + u_{1,i}\cos\theta_i \\ \theta_{i-1} + u_{2,i} \end{bmatrix}}^{\mathrm{f(x_{i-1},u_i)}\in\mathbb{R}^3}, \overbrace{\begin{bmatrix} u_{1,i} \\ u_{2,i} \end{bmatrix}}^{\mathrm{u_i}\in\mathbb{R}^2} = \begin{bmatrix} {}^s\Delta_{c,i} + \delta_{s,i} \\ {}^\theta\Delta_{c,i} + \delta_{\theta,i} \end{bmatrix}, \tag{28}$$

and

$$\overbrace{\begin{bmatrix} {}^s\Delta_{c,i} \\ {}^\theta\Delta_{c,i} \end{bmatrix}}^{\Delta_i\in\mathbb{R}^2} = \begin{bmatrix} \dfrac{{}^s\Delta_{r,i} + {}^s\Delta_{l,i}}{2} & \dfrac{{}^s\Delta_{r,i} - {}^s\Delta_{l,i}}{L} \end{bmatrix}^{\mathrm{T}}, \tag{29}$$

[5]Effectiveness of two-stage controller can be appreciated in the following video: https://youtu.be/0EAvl1veC-o.

[6]Models (28)-(30) are a discrete approximation of the continuous model (1), in function of the traveled linear distance by both lateral wheels. $i = 1, 2, \ldots$ is used in this paper as the discrete variable.

where $\delta_\Delta = [\delta_{s,i}\ \delta_{\theta,i}]^{\mathrm{T}}$ is the gaussian-assumed noise vector, which disturbs the distance and angle increments vector $\left[{}^{s}\Delta_{c,i}\ {}^{\theta}\Delta_{c,i}\right]^{\mathrm{T}}$ that robot effectuates in the interval $(i-1, i)$, whose input variables are in function of the linear circular displacements of right ${}^{s}\Delta_{r,i}$ and left ${}^{s}\Delta_{l,i}$ wheels. Eventually, a measurement model at the output is also considered as

$$\mathrm{y_i} = \overbrace{\begin{bmatrix} x_i + \delta_{x,i} \\ y_i + \delta_{y,i} \end{bmatrix}}^{\mathrm{h(y_i)}\in\mathbb{R}^2}, \tag{30}$$

where $\delta_{x,i}$ and $\delta_{y,i}$ are also gaussian-assumed noise signals, that invade to the measured variables x_i and y_i. These models are necessarily used to represent the kinematics of the robot, and to formulate the following estimator EKF.

Proposition 3 (Extended Kalman filter): The optimal estimation of position $(\hat{x}_i, \hat{y}_i)$ and orientation $(\hat{\theta}_i)$ for system (28)-(30), are obtained through the following non-linear observer:

$$\hat{\mathrm{x}}_\mathrm{i} = \mathrm{f}\left(\hat{\mathrm{x}}_{\mathrm{i}-1}, \mathrm{u_i}\right) + \mathrm{l_i}\left(\mathrm{y_i} - \hat{\mathrm{y}}_\mathrm{i}\right), \tag{31}$$

$$\hat{\mathrm{y}}_\mathrm{i} = \mathrm{h}\left(\hat{\mathrm{x}}_\mathrm{i}\right) = \begin{bmatrix} \hat{x}_i & \hat{y}_i \end{bmatrix}^{\mathrm{T}}, \tag{32}$$

where $\hat{\mathrm{x}}_\mathrm{i} = [\hat{x}_i\ \hat{y}_i\ \hat{\theta}_i]^{\mathrm{T}}$ is the estimation vector, and $\mathrm{l_i}$ is the applied Kalman gain to the observer. Then, the observer forces the estimation error trajectories $\tilde{\mathrm{e}}_\mathrm{i} = \mathrm{x_i} - \hat{\mathrm{x}}_\mathrm{i}$ to converge towards a small vicinity of zero where it remain ultimately bounded as $t \to \infty$, due to the Kalman gain, which depends on procedure stated below.

Given that model (28) can be approximated as

$$\mathrm{x_i} \approx \mathrm{F_i x_{i-1}} + \mathrm{G_i \Delta_i} + \mathrm{G_i Q_i}, \tag{33}$$

$$\mathrm{y_i} \approx \mathrm{H_i x_i} + \mathrm{H_i R_i}, \tag{34}$$

with the jacobian matrices

$$\mathrm{F_i} = \frac{\partial \mathrm{f}\left(\hat{\mathrm{x}}_{\mathrm{i}-1}, \mathrm{u_i}\right)}{\partial \mathrm{x}_{\mathrm{i}-1}},\ \mathrm{G_i} = \frac{\partial \mathrm{f}\left(\hat{\mathrm{x}}_{\mathrm{i}-1}, \mathrm{u_i}\right)}{\partial \mathrm{u_i}} \text{ and } \mathrm{H_i} = \frac{\partial \mathrm{h}\left(\hat{\mathrm{y}}_\mathrm{i}\right)}{\partial \mathrm{y_i}}, \tag{35}$$

another matrix

$$\mathrm{Q_i} = \begin{bmatrix} \left(\alpha_1|u_{1,i}| + \alpha_2|u_{2,i}|\right)^2 & 0 \\ 0 & \left(\alpha_3|u_{1,i}| + \alpha_4|u_{2,i}|\right)^2 \end{bmatrix}, \tag{36}$$

where noise energy is bounded within the motion model (33), and matrix

$$\mathrm{R_i} = \begin{bmatrix} \sigma_m^2 & 0 \\ 0 & \sigma_m^2 \end{bmatrix}, \tag{37}$$

inwhich variance information of gaussian noise in measured variables x_i and y_i are contained. Then, Kalman gain is determined by the following calculations:

1) Prediction of covariance matrix $\bar{\Sigma}_\mathrm{i}$[7]:

$$\bar{\Sigma}_\mathrm{i} = \mathrm{F_i}\Sigma_{\mathrm{i}-1}\mathrm{F_i^T} + \mathrm{G_i Q_i G_i^T}. \tag{38}$$

2) Innovation covariance matrix $\mathrm{S_i}$:

$$\mathrm{S_i} = \mathrm{H_i}\bar{\Sigma}_\mathrm{i}\mathrm{H_i^T} + \mathrm{R_i}. \tag{39}$$

3) Kalman gain $\mathrm{l_i}$:

$$\mathrm{l_i} = \bar{\Sigma}_\mathrm{i}\mathrm{H_i^T}\mathrm{S_i^{-1}}. \tag{40}$$

[7] $\mathrm{Q_i}$ is mapped to the space of Σ_i by $\mathrm{G_i}$

4) Correction of covariance matrix Σ_i:

$$\Sigma_\mathrm{i} = \left(\mathrm{I} - \mathrm{l_i H_i}\right)\bar{\Sigma}_\mathrm{i}. \tag{41}$$

Proof 3: See [11], [12]. □

Fig. 9 illustrates the implementation of extended Kalman filter, whose procedure assumes an equal variance $\sigma_m^2 = 0.2$ for noise in measured variables $\{x_i, y_i\}$ and an established boundedness by $\alpha_1 = 2\mathrm{E}-3$, $\alpha_2 = 1\mathrm{E}-2$, $\alpha_3 = 1\mathrm{E}-2$ and $\alpha_4 = 1\mathrm{E}-3$ for noise at inputs $\{u_{1,i}, u_{2,i}\}$.

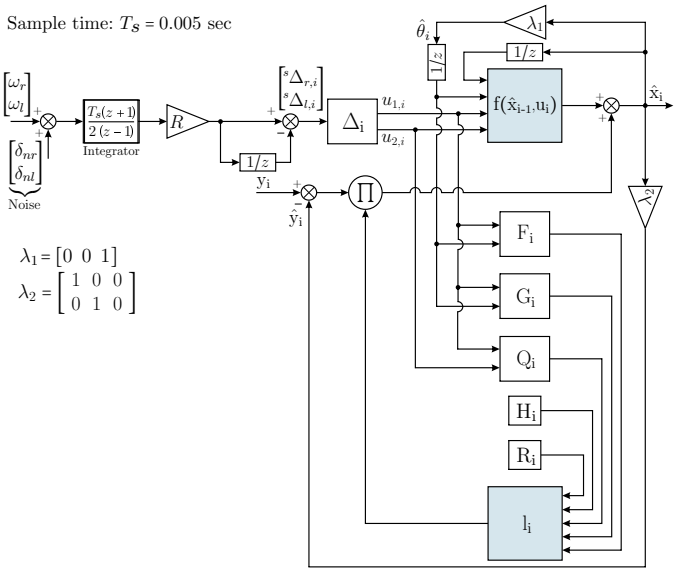

Fig. 9: EKF Scheme. Angular velocities $\{\omega_r, \omega_l\}$ and location $\{x, y\}$ are received as input variables and used for computing the estimation $\hat{\theta}$.

IV. Time-gap Leader-follower formation (TLF)

Given that our main aim is to built a set of leader-follower reference trajectories based on time-gap synchronization for a n-robot system (see Fig. 10), then, a methodology is proposed so that a leader robot $\{1\}$ will command the navigation mission by tracking a desired reference r, while the rest of each involved follower robot $\{m\}$ $(m = \{2, 3, \ldots, n\})$ will track the trajectory p generated by its predecessor $\{m-1\}$, with an available time-gap separation.

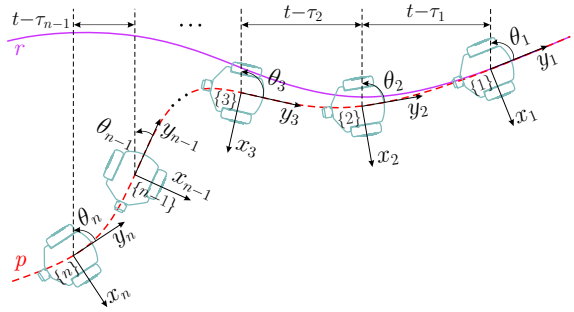

Fig. 10: Leader-follower scheme with time-gap separation.

In this methodology, it is firstly considered an existing dynamics that governs the delayed behavior of each robot $\{g=m-1\}$ as follows:

$$ {}^{\tau_g}\dot{q}_g = \begin{bmatrix} \dot{x}_g(t-\tau_g) \\ \dot{y}_g(t-\tau_g) \\ \dot{\theta}_g(t-\tau_g) \end{bmatrix} = \overbrace{\begin{bmatrix} -u_{1g}(t-\tau_g)\sin\theta_g(t-\tau_g) \\ u_{1g}(t-\tau_g)\cos\theta_g(t-\tau_g) \\ u_{2g}(t-\tau_g) \end{bmatrix}}^{\mathcal{F}({}^{\tau_g}q_g,\,{}^{\tau_g}u_g)}, \quad (42) $$

where $u_{1g}(t-\tau_g)$, $u_{2g}(t-\tau_g)$ and $\theta_g(t-\tau_g)$ are the input velocities and orientation of $\{g\}$ with a time-delay τ_g. Responses of (42) can be perfectly estimated via a non-linear observer and associated to $\{m\}$ through their initial conditions, to be posteriorly used as reference trajectories of two-stage controllers. Then, under the following additional assumption, a non-linear observer is proposed below in Proposition 4.

Assumption 3: Delayed state ${}^{\tau_g}q_g=[x_g(t-\tau_g)\ y_g(t-\tau_g)\ \theta_g(t-\tau_g)]^{\mathrm{T}}$, and delayed kinematic input ${}^{\tau_g}u_g=[u_{1g}(t-\tau_g)\ u_{2g}(t-\tau_g)]^{\mathrm{T}}$ of each $\{g\}$ are available for whichever design purpose.

Proposition 4 (Delayed dynamics observer): According to model (42), the correct estimation of delayed state ${}^{\tau_g}\hat{q}_g = [\hat{x}_g(t-\tau_g)\ \hat{y}_g(t-\tau_g)\ \hat{\theta}_g(t-\tau_g)]^{\mathrm{T}}$ of each $\{g\}$ are obtained through the following non-linear observer[8]:

$$ {}^{\tau_g}\dot{\hat{q}}_g = \mathcal{F}({}^{\tau_g}\hat{q}_g, {}^{\tau_g}u_g) + \Gamma_g[{}^{\tau_g}q_g - {}^{\tau_g}\hat{q}_g], \quad (43) $$

which represents a copy of system (42), but as a function of the estimated delayed orientation $\hat{\theta}_g(t-\tau_g)$ and the estimation error vector ${}^{\tau_g}e_{q_g} = ({}^{\tau_g}q_g - {}^{\tau_g}\hat{q}_g)$. Vector $\Gamma_g = [b_{1g}\ b_{2g}\ b_{3g}]^{\mathrm{T}}$ of positive gains forces the trajectories of ${}^{\tau_g}e_{q_g}$ to converge towards a small vicinity of zero where they remain ultimately bounded as $t\to\infty$ and this vicinity can be reduced as much as gains vector β_g is permissibly increased.

Proof 4: Let be ${}^{\tau_g}e_{x_g}=x_g(t-\tau_g)-\hat{x}_g(t-\tau_g)$, ${}^{\tau_g}e_{y_g}=y_g(t-\tau_g)-\hat{y}_g(t-\tau_g)$, and ${}^{\tau_g}e_{\theta_g}=\theta_g(t-\tau_g)-\hat{\theta}_g(t-\tau_g)$ the estimation errors of (43), and they are conveniently expressed at the delayed body frames $\{x_g(t-\tau_g), y_g(t-\tau_g)\}$ as follows:

$$ \begin{bmatrix} z_{1g} \\ z_{2g} \\ z_{3g} \end{bmatrix} = \begin{bmatrix} -\sin\theta_g(t-\tau_g) & \cos\theta_g(t-\tau_g) & 0 \\ \cos\theta_g(t-\tau_g) & \sin\theta_g(t-\tau_g) & 0 \\ 0 & 0 & 1 \end{bmatrix} \begin{bmatrix} {}^{\tau_g}e_{x_g} \\ {}^{\tau_g}e_{y_g} \\ {}^{\tau_g}e_{\theta_g} \end{bmatrix}. \quad (44) $$

Now, estimation error dynamics of each $\{g\}$ are obtained by computing the time derivative of (44), which yields

$$ \dot{z}_{1g} = -z_{2g}u_{2g}(t-\tau_g) + u_{1g}(t-\tau_g)[1-\cos z_{3g}] - bz_{1g}, \quad (45) $$

$$ \dot{z}_{2g} = z_{1g}u_{2g}(t-\tau_g) - u_{1g}(t-\tau_g)\sin z_{3g} - bz_{2g}, \quad (46) $$

$$ \dot{z}_{3g} = -bz_{3g}, \quad (47) $$

with $b_{1g}=b_{2g}=b_{3g}=b>0$. Note that (47) is exponentially stable, furthermore $u_{1g}(t-\tau_g)[1-\cos z_{3g}\ \ -\sin z_{3g}]^{\mathrm{T}}$ converges to zero as fast as parameter b is increased, and the problem is reduced to prove asymptotic stability on

$$ \dot{z}_{1g} = -z_{2g}u_{2g}(t-\tau_g) - bz_{1g}, \quad (48) $$

$$ \dot{z}_{2g} = z_{1g}u_{2g}(t-\tau_g) - bz_{2g}. \quad (49) $$

[8]State ${}^{\tau_g}q_g$ is obtained here by delaying the signals that EKF provides.

It is easy to see that by selecting $V_2=(z_{1g}+z_{2g})^2/2$ as a candidate Lyapunov function, its time-derivative $\dot{V}_2 = -bz_{1g}^2 - bz_{2g}^2$ results negative definite, which guarantees asymptotic stability around the unique equilibrium point $\mathcal{C}=[0\ 0\ 0]^{\mathrm{T}}$ of (45)-(47), which concludes this proof. □

Programmed observer in $\{m\}$ ensures the tracking of delayed behavior of $\{g\}$ from its initial pose[9], and originated responses serve as the reference of its two-stage controller as follows:

$$ \begin{aligned} &x_m^*=\hat{x}_g(t-\tau_g),\ \ y_m^*=\hat{y}_g(t-\tau_g),\ \ \theta_m^*=\hat{\theta}_g(t-\tau_g), \\ &u_{1m}^*=\sqrt{\dot{\hat{x}}_g(t-\tau_g)^2+\dot{\hat{y}}_g(t-\tau_g)^2},\ \text{and}\ u_{2m}^*=\dot{\hat{\theta}}_g(t-\tau_g). \end{aligned} \quad (50) $$

Finally, a smoothing discrete function $\wp$ was placed in series with the observer's integral action to overcome the effect of peaking phenomena caused by maximum estimation errors at initial run-time seconds. So, $\wp$ yields

$$ \wp(iT_s) = \begin{cases} \frac{1}{2}\left(1-\cos\frac{\pi}{5}iT_s\right) & \text{if}\ \ iT_s<5\ \text{sec}, \\ 1 & \text{if}\ \ iT_s\geq 5\ \text{sec}. \end{cases} \quad (51) $$

This TLF uses $b_{1g}=b_{2g}=b_{3g}=3$ in the simulations of Section V, and successful results are exhibited together with the implementation of the two-stage controller.

V. Simulation results

Two dynamic simulations (integrating ADAMS with MATLAB) are presented here to validate the robustness of the two-stage controller, and the correct functionality of the proposed leader-follower formation. In the first simulation a "∞" shape trajectory is used as reference of robot $\{1\}$, which is described by following expressions:

$$ \begin{aligned} &x^* = 2\text{E}3\sin(t/8) + x^*(0),\ x^*(0) = 2.5\text{E}3\ \text{mm}, \\ &y^* = 2\text{E}3\sin(t/4) + y^*(0),\ y^*(0) = 2.5\text{E}3\ \text{mm}. \end{aligned} \quad (52) $$

Thus, Fig. 11(a) shows an adequate tracking of this reference made by three robots that use a leader-follower formulation, with a time-gap of 5 seconds. It is interesting to notice how they get closer or farther away at different intervals to regulate this time delay[10].

Now, similarly to the first simulation, five robots are commanded in a second simulation to track a four-petal flower shape reference, characterized by the following equations:

$$ \begin{aligned} &x^*=2.5\text{E}3\cos(\pi t/30)\sin(\pi t/60)+x^*(0),\ x^*(0)=5\text{E}3\ \text{mm}, \\ &y^*=-2\text{E}3\cos(\pi t/30)\cos(\pi t/60)+y^*(0),\ y^*(0)=4\text{E}3\ \text{mm}. \end{aligned} \quad (53) $$

Dynamics of all robots in this simulation are shown in Fig. 11(d), where each vehicle executes an appropriate tracking of the reference trajectory left by its predecessor, with the same time-gap of the first simulation. In addition, it is clearly perceptible that the proposed two-stage controller is effective according to stability and regulation objectives. Regarding

[9]Observer integrator must be settled with the initial conditions of involved follower robot.

[10]Additionally, several simulations of TLF can be found in the following video: https://youtu.be/WqMPkJ7GrcY.

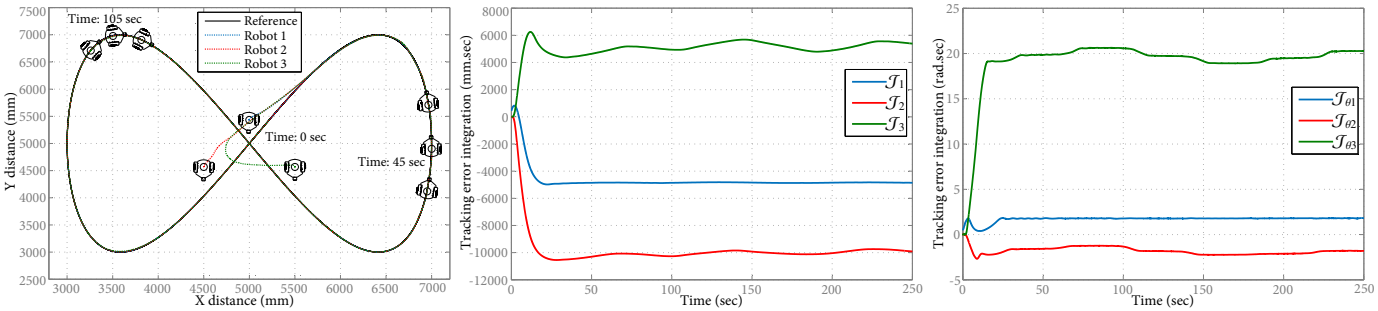

(a) Evolution of 3-robot system in first simulation. (b) Evolution of distance functionals. (c) Evolution of orientation functionals.

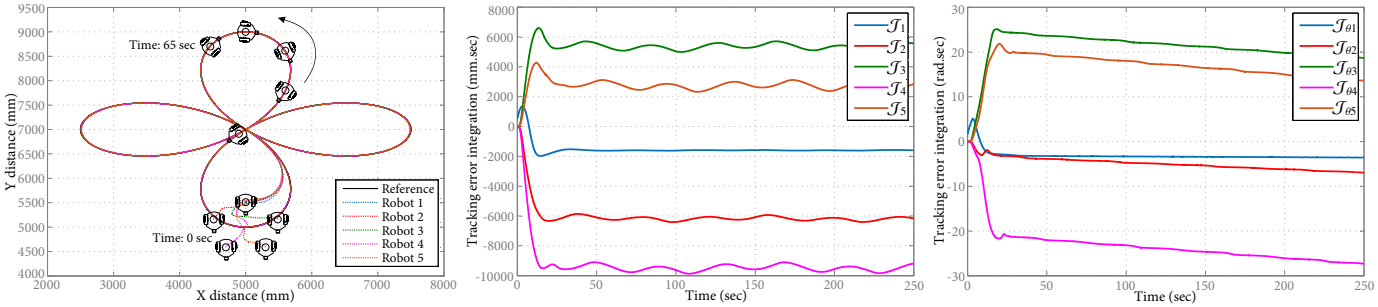

(d) Evolution of 5-robot system in second simulation. (e) Evolution of distance functionals. (f) Evolution of orientation functionals.

Fig. 11: Controlled navigation of 3-robot and 5-robot systems.

control system performance, tracking error functionals were computed as:

$$\mathcal{J}_z = \int_0^t [(x_z - x_z^*) + (y_z - y_z^*)]dt \text{ and } \mathcal{J}_{\theta z} = \int_0^t (\theta_z - \theta_z^*)dt, \quad z = 1, 2, \ldots, n, \tag{54}$$

for evaluating how good the behavior of each mobile robot is in the tracking mission. Then, the evolution of $\mathcal{J}_z$ and $\mathcal{J}_{\theta z}$ are respectively exhibited in Fig. 11(b), Fig. 11(c), Fig. 11(e) and Fig. 11(f) for both simulations. Under ideal conditions, a constant value trend is expected for the computed functionals, however, friction, slip disturbances and other unconsidered dynamics cause the undesired time-variant and oscillatory behavior shown after 20 seconds, when tracking error values are minimum.

VI. Conclusions

Developed simulations demonstrated that the two-stage controller is robust and effective in the tracking of trajectories for differential-drive wheeled mobile robot. Control law ϱ in TC was efficient rejecting disturbances caused by wheels' slipping when in motion. The dynamics of these disturbances were in principle assumed as unknown, and TC allowed to reject them with only a prior knowledge of their boundedness value ($\|\delta\|_\infty$), which results useful with respect to other control strategies. Additionally, EKF achieved an adequate estimation of θ, which is indispensable in TC stage, and results indicate that EKF does not compromise the closed-loop stability. AVC together with a loop-shaping tuning method guarantee a wide range of frequencies with robust stability and performance in the closed-loop system. Simulations validate the correct tuning of this controller and the appropriate selection of weighting functions to bound the associated uncertainties and disturbances to the first stage.

Finally, the synchronized navigation under TLF is an interesting formulation that facilitates the creation of references for each member in the formation. Moreover, whole control system is a decentralized strategy, where the motion of any robot depends only on that of its predecessor. The proposed system could additionally be augmented with a supervisory system to prevent inter-robot collisions at the initial run-time seconds. In a future work, it would be attractive to explore TLF in other kind of robots such as unmanned aerial vehicles (UAVs).

References

[1] S. Suzuki. Recent researches on innovative drone technologies in robotics field. *Advanced Robotics*, 32(19):1008–1022, 2018.

[2] Daniel K. D. Villa, Alexandre S. Brandão, and Mário Sarcinelli-Filho. A survey on load transportation using multirotor UAVs. *Journal of Intelligent & Robotic Systems*, Oct 2019.

[3] T. Adamek, C. A. Kitts, and I. Mas. Gradient-based cluster space navigation for autonomous surface vessels. *IEEE/ASME Transactions on Mechatronics*, 20(2):506–518, Apr 2015.

[4] G. L. Mariottini, F. Morbidi, D. Prattichizzo, N. Vander Valk, N. Michael, G. Pappas, and K. Daniilidis. Vision-based localization for leader–follower formation control. *IEEE Transactions on Robotics*, 25(5):1431–1438, Dec 2009.

[5] Khalil Alipour, Arsalan Babaei Robat, and Bahram Tarvirdizadeh. Dynamics modeling and sliding mode control of tractor-trailer wheeled mobile robots subject to wheels slip. *Mechanism and Machine Theory*, 138:16–37, Aug 2019.

[6] Mauro Baquero-Suárez, John Cortes-Romero, Jaime Arcos-Legarda, and Horacio Coral-Enriquez. Estabilización Automática de una Bicicleta sin Conductor mediante el Enfoque de Control por Rechazo Activo de

Perturbaciones. *Revista Iberoamericana de Automática e Informática industrial*, 15(1):86–100, 2017.

[7] Mauro Baquero-Suárez, John Cortes-Romero, Jaime Arcos-Legarda, and Horacio Coral-Enriquez. A Robust Two-stage Active Disturbance Rejection Control for the Stabilization of a Riderless Bicycle. *Multibody System Dynamics*, 45(1):7–35, 2019.

[8] Lennart Ljung. *System Identification, Theory for the User*, chapter 6, pages 168–196. Prentice Hall PTR, second edition, 1999.

[9] Horacio Coral-Enriquez, Santiago Pulido-Guerrero, and John Cortés-Romero. Robust Disturbance Rejection Based Control with Extended-state Resonant Observer for Sway Reduction in Uncertain Tower-cranes. *International Journal of Automation and Computing*, 2019.

[10] M.H. Shafiei and F. Monfared. Design of a Robust Tracking Controller for a Nonholonomic Mobile Robot with Side Slipping based on Lyapunov Redesign and Nonlinear H∞ Methods. *Systems Science & Control Engineering*, 7(1):1–11, 2019.

[11] Frank L. Lewis, Lihua Xie, and Dan Popa. *Optimal and Robust Estimation, with an Introduction to Stochastic Control Theory*, chapter 5, pages 259–304. CRC Press, Taylor and Francis Group, second edition, 2008.

[12] Shiyuan Wang, Wanli Wang, Badong Chen, and Chi K. Tse. Convergence analysis of nonlinear Kalman filters with novel innovation-based method. *Neurocomputing*, 289:188–194, Feb 2018.